Radiotherapy and Oncology 115 (2015) 186–190

Contents lists available at ScienceDirect

Radiotherapy and Oncology

journal homepage: www.thegreenjournal.com

Prostate tumor delineation

Prostate tumor delineation using multiparametric magnetic resonance imaging: Inter-observer variability and pathology validation

Peter Steenbergen [a], Karin Haustermans [c], Evelyne Lerut [e], Raymond Oyen [d], Liesbeth De Wever [d], Laura Van den Bergh [c], Linda G.W. Kerkmeijer [f], Frank A. Pameijer [g], Wouter B. Veldhuis [g], Jochem R.N. van der Voort van Zyp [f], Floris J. Pos [a], Stijn W. Heijmink [b], Robin Kalisvaart [a], Hendrik J. Teertstra [b], Cuong V. Dinh [a], Ghazaleh Ghobadi [a], Uulke A. van der Heide [a,*]

[a] Department of Radiation Oncology; [b] Department of Radiology, The Netherlands Cancer Institute, Amsterdam, The Netherlands; [c] Radiation Oncology, University Hospitals Leuven, Department of Oncology, KU Leuven; [d] Radiology; [e] Pathology, University Hospitals Leuven, Department of Imaging & Pathology, KU Leuven, Belgium; [f] Department of Radiation Oncology; and [g] Department of Radiology, University Medical Center Utrecht, The Netherlands

ARTICLE INFO

Article history:
Received 13 October 2014
Received in revised form 27 March 2015
Accepted 19 April 2015
Available online 29 April 2015

Keywords:
Prostate cancer
Radiotherapy
Tumor delineation
Multiparametric MRI
Dose escalation
Inter-observer variability

ABSTRACT

Background and purpose: Boosting the dose to the largest (dominant) lesion in radiotherapy of prostate cancer may improve treatment outcome. The success of this approach relies on the detection and delineation of tumors. The agreement among teams of radiation oncologists and radiologists delineating lesions on multiparametric magnetic resonance imaging (mp-MRI) was assessed by measuring the distances between observer contours. The accuracy of detection and delineation was determined using whole-mount histopathology specimens as reference.

Material and methods: Six observer teams delineated tumors on mp-MRI of 20 prostate cancer patients who underwent a prostatectomy. To assess the inter-observer agreement, the inter-observer standard deviation (SD) of the contours was calculated for tumor sites which were identified by all teams.

Results: Eighteen of 89 lesions were identified by all teams, all were dominant lesions. The median histological volume of these was 2.4 cm^3. The median inter-observer SD of the delineations was 0.23 cm. Sixty-six of 69 satellites were missed by all teams.

Conclusion: Since all teams identify most dominant lesions, dose escalation to the dominant lesion is feasible. Sufficient dose to the whole prostate may need to be maintained to prevent under treatment of smaller lesions and undetected parts of larger lesions.

Boosting the radiation dose to the visible cancer inside the prostate may improve treatment outcome. This theory is motivated by the observation that prostate cancer often recurs at the site of the dominant lesion [1,2] and by observations that escalating the radiation dose improves treatment outcome [3]. A boost to the largest lesion in the prostate (the dominant lesion), in addition to a standard dose to the whole organ may achieve adequate dose escalation without increasing toxicity [4,5]. This hypothesis is currently tested in a phase III clinical trial, the FLAME trial [6]. Boost volumes can be defined on multiparametric magnetic resonance imaging (mp-MRI).

Mp-MRI, consisting of a combination of T2-weighted (T2w), diffusion-weighted (DWI) and dynamic contrast enhanced (DCE) images, has a high diagnostic accuracy for detection of prostate cancer [7,8]. By dividing the gland into regions and scoring tumor presence per region, specificities and sensitivities for tumor detection in the range of 0.53–0.81 and 0.80–0.96 are feasible [9]. Sensitivity using all three modalities together is higher than for the separate modalities [10].

The inter-observer agreement of tumor detection can be quantified using a kappa statistic. The number of volume elements (regions of the prostate or voxels in the images) for which the observers agree is expressed as a value ranging from zero (no agreement) to one (perfect agreement). Studies of region-based tumor detection on mp-MRI have reported kappa values ranging from 0.40 to 0.63 [11,12]. Rischke et al. [13] performed a kappa analysis on a voxel-by-voxel basis in five patients. They compared tumor delineations of five observers with delineations by a reference observer, resulting in an agreement of 0.51 ± 0.15 (mean ± standard deviation; range 0.22–0.73) for a combination

* Corresponding author at: The Netherlands Cancer Institute, Department of Radiation Oncology, Plesmanlaan 121, 1066 CX Amsterdam, The Netherlands.
E-mail address: u.vd.heide@nki.nl (U.A. van der Heide).

http://dx.doi.org/10.1016/j.radonc.2015.04.012
0167-8140/

of T2w and DWI images and 0.63 ± 0.12 (range 0.00–0.80) for T2w with DCE images. Delineation on a combination of all three MR sequences was not studied by these authors. Anwar et al. compared delineations by two observers on T2w imaging and MR spectroscopy with delineations on histology and found these to differ by a median distance of 1.4 mm [14].

In this study, we determine the inter observer agreement and geometrical distances between the contours of the observers. The latter is the measure closest to the delineation practice in radiotherapy. Six teams from three different centers were recruited, each team consisting of a radiation oncologist and a radiologist, which delineated prostate tumors on mp-MRI. By comparing the results with histology, we assessed to what extent tumors were correctly identified and what the agreement was between the observer and pathology contours.

Methods

Dataset

Twenty patients with biopsy proven prostate cancer were selected who consulted the Department of Radiation Oncology of the University Hospitals Leuven. The patients were prospectively included in an earlier study [10,15]. Between February 2008 and February 2011 they underwent an mp-MRI exam before prostatectomy. The patients were selected such that the majority had T2c or T3a prostate cancer based on analysis of the prostatectomy specimens. Apart from tumor stage, the selection was random. Written informed consent was obtained from all patients.

The mp-MRI scan consisted of T2-weighted (T2w), diffusion weighted (DWI), and dynamic contrast-enhanced (DCE) scans. These were acquired on 1.5T MR scanner (SonataVision, SymphonyVision or Aera, Siemens Erlangen, Germany) using a combination of a six-channel phased-array body coil and a spine coil. Because the patients were selected retrospectively, the scanning parameters varied (see Supplementary material). Orthogonal transversal, coronal and sagittal T2w scans were acquired. ADC maps were calculated from the DWI scan by the scanner software. For the DCE scans, the contrast agent (Dotarem, Guerbet, France, 15 ml) was injected at the fourth dynamic scan with a rate of 2 ml/s, followed by a 20 ml saline flush. The signal intensities were first converted to gadolinium concentration values [16] using reference T1 values [17]. The extended Tofts model was fitted to the concentration time curves for estimation of the volume transfer constant (K^{trans}) using the method by Murase [18] with a population-based arterial input function.

Six teams of delineators were recruited from three hospitals (two teams per hospital). Each team consisted of a radiation oncologist and a radiologist. Using the mp-MRI, they delineated the visible tumors on the transversal T2 (T2t) scan. To assure that the study results are representative for a realistic clinical situation, the teams used the delineation system of their own hospital. The teams were provided with biopsy information, TRUS findings and written radiology reports. The final delineations were approved by both members of the team.

Pathology

Whole-mount histological slices were cut from the prostatectomy specimens perpendicular to the urethra at 3–4 mm intervals [10,15]. From these, Hematoxylin-eosin (H&E) stained whole-mount pathology slides were obtained on which a single pathologist delineated the tumors. The H&E slides were registered to the T2t image to allow assessment of tumor detection accuracy of the observers. First, each pathology slide was assigned to a T2t slice based on the relative order of the H&E slides, the location of apex and base, size of the subsequent slices in MRI and pathology and the distance between the slides (3 or 3.3 mm in T2t, 3–4 mm in histology). For some T2t slices no H&E slice was present due to the difference in slice distance. The location of the pathology slides does not necessarily coincide with the location of the MRI slices. Therefore the true location of an H&E slice in the T2t scan can be somewhere between two slices. The T2t slice distance is 3.3 mm for most patients; assuming that the best matching T2w slice is selected, the average error is 0 mm, ranging from −1.65 to +1.65 mm. The average absolute error in the slice direction is then 0.8 mm.

Subsequently, each slice was registered by means of a deformable point-based method (Coherent Point Drift) using landmark points which were visible on both images. These were mostly based on the prostate boundary and occasionally other features, such as the ends of the peripheral zone and transitions between prostate and seminal vesicles. We estimated the registration error by selecting one landmark not used for registration per pathology slice and measuring the distance between this point on T2t MRI and registered pathology. The average error we found was 2.1 mm; the largest error was 5 mm. We could not assess the error resulting from possible differences in orientation of the pathology slices and the imaging.

The pathologist delineated the tumor locations on the H&E slices prior to registration. These delineations were digitized after image registration. The contours of seven dominant lesions and one satellite were interpolated for slices where no matching H&E slice was present while a tumor was found at the same site in both the previous and next slice.

Analysis

All contour analyses were done by one author using each patient's T2t scan grid as unit of analysis. The contours of the same site by different teams were grouped manually based on overlap. Depending on whether or not a corresponding pathology contour was found in the histology, the contour groups were counted as true positives, false positives and false negatives. Delineations made on MRI slices without matching histology were categorized as unconfirmed.

The prostate voxels were divided in healthy/tumor based on pathology and in true/false positive/negative based on pathology and consensus detections by all teams. The median and quartile of the voxel values of these categories were calculated for all scans. For this, all images were first normalized to their median.

The volumes of the observer delineations were estimated by counting the number of T2t voxels in the contours and multiplying this by the voxel volume. The same was done for the digitized pathologist's contours. Differences between teams in delineated volumes were analyzed using the Friedman test in Matlab (version 8.1, Statistics Toolbox 8.2, Natick, Massachusetts: The MathWorks Inc., 2013), with the observer teams as factor and patients as "nuisance factor".

The inter-observer delineation variation of the tumor sites which were delineated by all teams was assessed relative to a reference contour. The measure of interest was the standard deviation of the contour distances. The exact shape of the reference contour is not important for this, as long as it is smooth and similar in shape to the contours to be tested. The pathologist's contours had irregular shapes in some cases, making them unsuitable as a reference. Instead, the median of the observer contours was used, which was obtained by converting each contour to a mask, adding the six masks, smoothing the result and contouring the 50% level. The perpendicular distances of all points of the reference contour to each observer contour were then calculated and pooled [19]. The standard deviation (SD) of this pool was then calculated to obtain the inter-observer variability for one tumor site.

To facilitate comparison of the study results with literature, we assessed the agreement at the voxel level using kappa indices. When applied to detection in voxels, this index is identical to the DICE index. For tumors detected by all six teams, all 15 pair-wise kappa statistics were calculated. The agreement between pathology contours and the team delineations was also quantified using the kappa statistic; all observer contours were compared to the corresponding tumor found on pathology.

Results

Table 1 shows the characteristics of the 20 patients included in the present study. Histological analysis of the whole mount prostatectomy specimens revealed tumor stages ranging from T2b to T3b and Gleason scores from 7 to 9. A total of 89 tumors were found in the histology, 22 were larger than 0.4 cm^3. The scan values of the healthy prostate tissue and tumor are presented in Table 2.

An example of delineations by the six teams at the site of a dominant lesion is shown in Fig. 1. In this example, all teams indicated the same tumor location but the delineated tumor boundaries differed. Both over- and underestimations of tumor boundaries were made by the teams.

Forty sites were identified by one or more teams, of which 22 were true positives. Nineteen sites were detected by all teams, 18 of which were true positives; the 19th was a satellite at a site for which no matching histopathology was available. All 18 true positives were dominant lesions. Of the 21 sites delineated by some but not all teams, 4 were true and 17 were false positives. The largest true positive was the dominant lesion of patient 18. Table 2 shows the scan values for the consensus detections.

The dominant lesion of patient 1 was missed by all teams. It was located in the ventral part of the central zone; the biopsy report, however, indicated one positive biopsy in the right half of the prostate, where no tumor was found in histology, and two positives biopsies in the left half, where pathology revealed only small satellites. Sixty-six of 69 satellites were missed by all teams.

The 18 correctly detected dominant lesions had a median histological volume of 2.4 cm^3 (range 0.9–10.5 cm^3). The median volume of the other 71 lesions was 0.02 cm^3. Four of these were larger than 0.4 cm^3. The missed dominant lesion of patient 1 had a volume of 1.9 cm^3. The dominant lesion of patient 18 was also missed, but had a volume of only 0.45 cm^3. Two satellite lesions had volumes of 0.9 $cm^3$and 0.79 cm^3 respectively; the other lesions had a smaller volume. The volumes delineated by each of the six teams are shown in Fig. 2; the median delineated volumes differ significantly between teams (Friedman's ANOVA: $X^2(5) = 43.02$, $p < 0.001$).

Fig. 3 presents the inter-observer SDs of the 18 commonly detected tumors. The median of these 18 SDs was 0.23 cm (range 0.13–0.62 cm); no dependence of tumor volume is visible. The inter-observer SD for the dominant lesion of patient 17 was much

Table 1
Patient data. The information in the first four columns was available to the observers; the information in the other columns was derived from the prostatectomy specimens. The biopsy information of left (L) and right (R) hemispheres is coded as: number of positive biopsies (total number of biopsies). In patients where the L/R labels are missing, only information about the total number of biopsies was available.

Patient	Clinical information (available to observers)			Pathology information (not available to observers)			
	Gleason score (biopsy)	T stage TRUS (fMRI)	Number of positive biopsy cores (total)	Gleason score	T stage	Volume of dominant lesion [cm^3]	Notes
1	3 + 3	T2c-T3b	L2(5)/R1(5)	4 + 4	T2c	1.88	Mostly located in central gland
2	3 + 4	T2a (T2c)	L1(5)/R2(5)	4 + 3	T2c	1.34	
3	3 + 4	T3a (T2a)	3(3)	3 + 4	T3a	1.72	Satellite of 0.71 cm^3
4	4 + 4	T2b-T3a (T2b)	L2(4)/R2(4)	4 + 3	T3a	0.94	
5	4 + 3	T3a (T3a)	L1(2)/R3(4)	4 + 3	T2c	1.54	
6	4 + 3	T3a (T3a)	L1(4)/R0(4)	4 + 3	T3a	2.23	
7	5 + 4	T2c (T2c)	L2(5)/R4(5)	4 + 3	T3a	2.43	Satellite of 1.00 cm^3
8	3 + 4 + 5	T2a (T3a)	L1(3)/R1(3)	4 + 4	T2c	1.22	
9	3 + 4	T3b (T3b)	2(2)	4 + 4	T3b	8.96	
10	4 + 3	T2–T3a (T3a)	L5(5)/R(5)	4 + 3	T3a	8.85	
11	4 + 3	T2b–T3a (T3b)	L3(4)/R0(4)	4 + 3	T3a	3.26	
12	4 + 4	T3b (T3a)	L0(3)/R0(3)	5 + 4	T3a	5.22	
13	4 + 3	T3a (T3a)	2(6)	4 + 3	T3a	3.84	
14	4 + 4	T3a (T3b–T4)	L1(5)/R3(5)	4 + 4	T3b	1.93	
15	4 + 4	(T3a)	L0(5)/R5(5)	4 + 4	T3a	6.67	
16	4 + 3	T3b (T3b)	L2(5)/R5(5)	4 + 4	T3b	10.52	
17	4 + 4	T2a (T2c)	L3(5)/R0(5)	4 + 4	T2c	2.32	
18	4 + 5	T2a (T2c)	L0(5)/R1(5)	4 + 5	T2b	0.45	
19	4 + 3	T3a (T3a)	L5(5)/R2(5)	3 + 4	T2c	3.16	
20	3 + 4	T3b (T2a)	3*	4 + 4	T2c	1.87	

* For this patient the total number of biopsies was not reported.

Table 2
Imaging values of prostate tumor and healthy tissue together with true/false positives and negatives of the observer detections inside the prostate. For the latter, only consensus voxels (i.e. all or no teams detected the voxels) were included. The imaging data were normalized per patient and per scan by dividing the data through the median value inside the prostate. The values are shown as median and quartile values of all normalized voxels of all patients.

		Pathology		Consensus detections			
		Positive	Negative	True positive	False positive	True negative	False negative
T2 normalized	Median	0.95	1.01	0.85	0.87	1.02	1.09
	Quartiles	[0.78–1.16]	[0.78–1.29]	[0.72–0.99]	[0.73–1.01]	[0.78–1.32]	[0.87–1.36]
K^{trans} normalized	Median	1.41	0.96	1.97	1.92	0.92	0.99
	Quartiles	[0.94–2.12]	[0.59–1.47]	[1.41–2.64]	[1.39–2.67]	[0.56–1.40]	[0.69–1.43]
ADC normalized	Median	0.86	1.01	0.73	0.76	1.02	1.00
	Quartiles	[0.72–1.02]	[0.89–1.13]	[0.64–0.84]	[0.67–0.90]	[0.91–1.34]	[0.86–1.13]

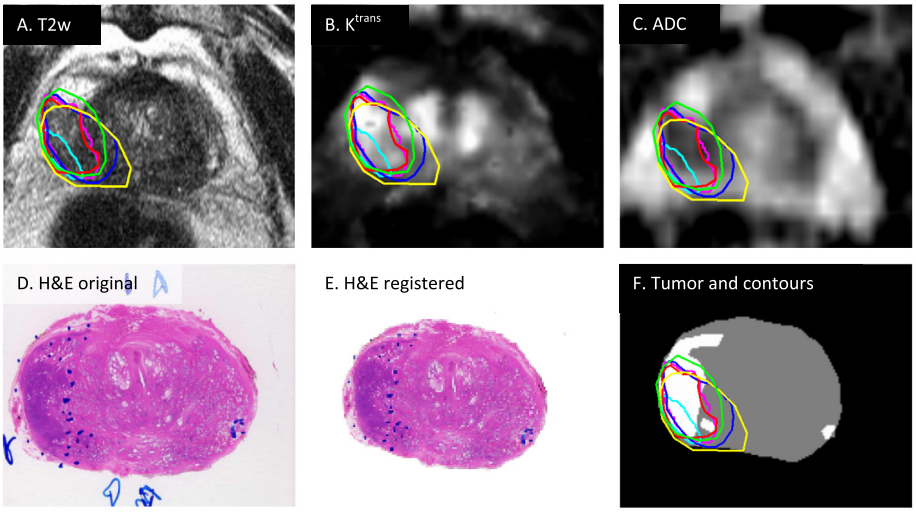

Fig. 1. (A–C) Example of delineations by the six teams on T2w, K^{trans} and ADC images. Panel D shows the corresponding H&E stained slice with the pathologist's contours in blue dots. Panel E shows the H&E slice registered to the T2w scan. Panel F shows delineations overlaid on the prostate in gray and tumor presence as determined by the pathologist in white.

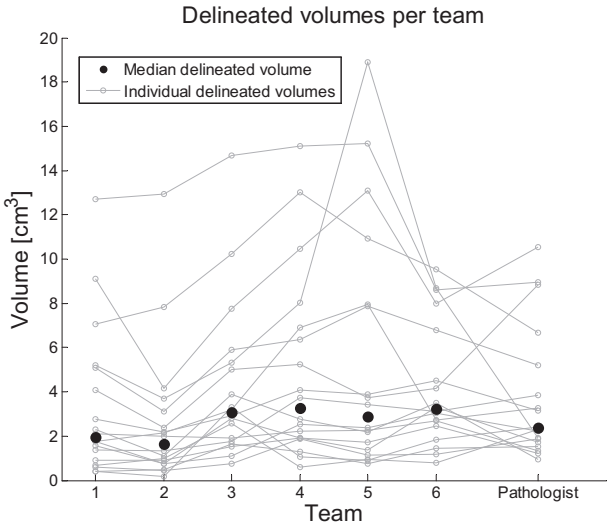

Fig. 2. Delineated volumes of the 18 tumors delineated by all teams and the pathologist. The gray markers are volumes for individual patients, with dotted lines connecting delineations in the same patient. The black markers are the median volumes for each team.

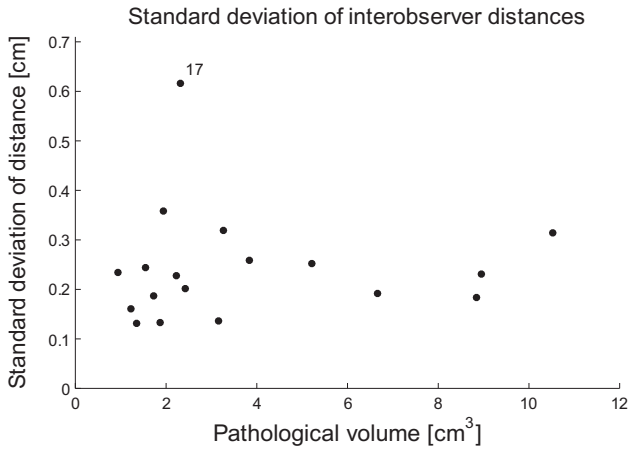

Fig. 3. Inter-observer standard deviations as function of pathological tumor volume. Patient 17 is discussed in the Results section.

higher than for the other patients because the contours were interlocking without being centered at the same location.

The kappa indices for the agreement between the delineations of the teams were 0.61 ± 0.19 (mean ± SD), ranging from 0 to 0.87. The kappa indices for the agreement between delineations of the teams and the pathologist were 0.45 ± 0.16, ranging from 0.08 to 0.74. This indicates that the agreement in delineation between teams was higher than the agreement between the teams and the pathologist's delineations on histology.

Discussion

We investigated the accuracy with which multiple teams detect and delineate prostate tumors on mp-MRI. The teams detected 18 of 22 tumors larger than 0.4 cm^3, all of which were dominant lesions. In two patients no dominant lesion was delineated by consensus. In one, the largest tumor identified by the pathologist was too small to be visible on MR. In the other case, the tumor delineated by the pathologist was sparse, meaning that it mostly consists of normal tissue interspersed with a large number of small lesions [20]. Since the central gland is heterogeneous by itself, this volume was not visible on MRI.

The teams differed in delineation of the tumor boundaries. For the delineated dominant lesions, the mean kappa value of 0.60 in our data is close to the value found by Rischke et al. [13]. The kappa statistic for agreement between observers and pathology was lower than the kappa between observers. This indicates that the observers to some extent delineate the same volumes and that they miss the same parts of the tumors. The missed parts of the tumor may be the consequence of these parts not being visible on MRI due to low Gleason score or sparsity of the tumor.

The difference in delineated volumes between teams suggests that some teams make more conservative estimates than others. This may be due to differences in interpretation of the images and to the importance that is attached to each of the MRI modalities. There is currently no consensus on optimal use of each of the series. Additional differences may occur depending on latent knowledge about treatment options and the wish to ensure that

the boost covers the tumor and therefore preferring wider tumor delineations in case of doubt.

The benefit of boosting may be limited by the accuracy of tumor delineation. This benefit will increase if the tumor delineations include more tumor tissue, which may be achieved by applying a margin to the delineated tumors. This expansion may be relatively small compared to margins for the whole gland since the dose fall-off from boost area to uniform dose will be shallow [21]. An alternative would be to increase the accuracy of delineation, for instance by increasing the visibility of tumors on MRI by improving scanning sequences or equipment or by training the observers to increase the consensus of delineation on mp-MRI. Additionally, consulting statistical model predictions on tumor presence [22,23] could provide helpful cues when delineating prostate tumors.

None of the seventeen false positives were delineated by all teams, suggesting that the information in the mp-MRI for these sites is ambiguous. Studying the properties of these areas of ambiguity may result in methods to provide single observers with cues about this uncertainty.

No tumors other than the dominant lesion were identified by all our teams, leaving 69 satellites undetected, most of which were smaller than 0.4 cm^3. The clinical relevance of satellite tumors in the prostate is currently a matter of debate. It has been suggested that these satellites do not require treatment since they show less hallmarks of cancer than the dominant lesions [24]. However, Huang et al. recently found small satellites to exhibit high Gleason patterns in 11% of their patients, which suggests that small foci do require treatment some cases [25]. For this reason, current boost trials maintain the dose to the organ outside the boost area at the regular clinical level.

Since patients were selected retrospectively, no special measures could be taken to optimize registration accuracy of histology on MRI. Some of the differences between the pathology and observer contours may be due to limited registration accuracy and the observer-to-pathology kappa statistic may therefore be biased downwards. Additionally, the pathology contours which we used as the gold standard are themselves due to inter observer variation. Volume estimates of small lesions which only appear in one slice are likely to be overestimated. The seminal vesicles and apex are not included in our histology stacks since they are handled separately by the pathology department; therefore volumes of tumors which extend toward the base or apical slice may be underestimated.

In conclusion, all teams consisting of a radiation oncologist and a radiologist found 18 of 20 verifiable dominant prostate lesions on mp-MRI. The inter-observer contour standard deviation for these tumors was 2.3 mm. The observers missed parts of the dominant lesions and all satellites, two of which were larger than 0.4 cm^3. A sufficient dose outside the boost volume should therefore be maintained to cover these missed volumes.

Conflict of interest statement

The authors have nothing to disclose.

Acknowledgement

This research was supported by the Dutch Cancer Society (NKI 2013-5937).

Appendix A. Supplementary data

Supplementary data associated with this article can be found, in the online version, at http://dx.doi.org/10.1016/j.radonc.2015.04.012.

References

[1] Cellini N, Morganti AG, Mattiucci GC, et al. Analysis of intraprostatic failures in patients treated with hormonal therapy and radiotherapy: implications for conformal therapy planning. Int J Radiat Oncol Biol Phys 2002;53:595–9.
[2] Pucar D, Hricak H, Shukla-Dave A, et al. Clinically significant prostate cancer local recurrence after radiation therapy occurs at the site of primary tumor: magnetic resonance imaging and step-section pathology evidence. Int J Radiat Oncol 2007;69:62–9.
[3] Viani GA, Stefano EJ, Afonso SL. Higher-than-conventional radiation doses in localized prostate cancer treatment: a meta-analysis of randomized controlled trials. Int J Radiat Oncol 2009;74:1405–18.
[4] Fonteyne V, Villeirs G, Speleers B, et al. Intensity-modulated radiotherapy as primary therapy for prostate cancer: report on acute toxicity after dose escalation with simultaneous integrated boost to intraprostatic lesion. Int J Radiat Oncol 2008;72:799–807.
[5] Singh AK, Guion P, Sears-Crouse N, et al. Simultaneous integrated boost of biopsy proven, MRI defined dominant intra-prostatic lesions to 95 Gray with IMRT: early results of a phase I NCI study. Radiat Oncol Lond Engl 2007;2:36.
[6] Lips IM, van der Heide UA, Haustermans K, et al. Single blind randomized Phase III trial to investigate the benefit of a focal lesion ablative microboost in prostate cancer (FLAME-trial): study protocol for a randomized controlled trial. Trials 2011;12:255.
[7] Barentsz JO, Richenberg J, Clements R, et al. ESUR prostate MR guidelines 2012. Eur Radiol 2012;22:746–57.
[8] Dickinson L, Ahmed HU, Allen C, et al. Magnetic resonance imaging for the detection, localisation, and characterisation of prostate cancer: recommendations from a European consensus meeting. Eur Urol 2011;59:477–94.
[9] De Rooij M, Hamoen EHJ, Fütterer JJ, Barentsz JO, Rovers MM. Accuracy of multiparametric MRI for prostate cancer detection: a meta-analysis. Am J Roentgenol 2014;202:343–51.
[10] Isebaert S, Van den Bergh L, Haustermans K, et al. Multiparametric MRI for prostate cancer localization in correlation to whole-mount histopathology. J Magn Reson Imaging 2013;37:1392–401.
[11] Bratan F, Niaf E, Melodelima C, et al. Influence of imaging and histological factors on prostate cancer detection and localisation on multiparametric MRI: a prospective study. Eur Radiol 2013;23:2019–29.
[12] Jung SI, Donati OF, Vargas HA, et al. Transition zone prostate cancer: incremental value of diffusion-weighted endorectal MR imaging in tumor detection and assessment of aggressiveness. Radiology 2013;269:493–503.
[13] Rischke HC, Nestle U, Fechter T, et al. 3 Tesla multiparametric MRI for GTV-definition of dominant intraprostatic lesions in patients with prostate cancer–an interobserver variability study. Radiat Oncol 2013;8:183.
[14] Anwar M, Westphalen AC, Jung AJ, et al. Role of endorectal MR imaging and MR spectroscopic imaging in defining treatable intraprostatic tumor foci in prostate cancer: quantitative analysis of imaging contour compared to whole-mount histopathology. Radiother Oncol 2014;110:303–8.
[15] Isebaert S, De Keyzer F, Haustermans K, et al. Evaluation of semi-quantitative dynamic contrast-enhanced MRI parameters for prostate cancer in correlation to whole-mount histopathology. Eur J Radiol 2012;81. e217–22.
[16] Schabel MC, Parker DL. Uncertainty and bias in contrast concentration measurements using spoiled gradient echo pulse sequences. Phys Med Biol 2008;53:2345–73.
[17] Fennessy FM, Fedorov A, Gupta SN, et al. Practical considerations in T1 mapping of prostate for dynamic contrast enhancement pharmacokinetic analyses. Magn Reson Imaging 2012;30:1224–33.
[18] Murase K. Efficient method for calculating kinetic parameters using T1-weighted dynamic contrast-enhanced magnetic resonance imaging. Magn Reson Med 2004;51:858–62.
[19] Steenbakkers RJHM, Duppen JC, Fitton I, et al. Observer variation in target volume delineation of lung cancer related to radiation oncologist–computer interaction: a "Big Brother" evaluation. Radiother Oncol 2005;77:182–90.
[20] Langer DL, van der Kwast TH, Evans AJ, et al. Intermixed normal tissue within prostate cancer: effect on MR imaging measurements of apparent diffusion coefficient and T2—sparse versus dense cancers 1. Radiology 2008;249:900–8.
[21] Lips IM, van der Heide UA, Kotte ANTJ, van Vulpen M, Bel A. Effect of translational and rotational errors on complex dose distributions with off-line and on-line position verification. Int J Radiat Oncol 2009;74:1600–8.
[22] Shah V, Turkbey B, Mani H, et al. Decision support system for localizing prostate cancer based on multiparametric magnetic resonance imaging. Med Phys 2012;39:4093–103.
[23] Vos PC, Barentsz JO, Karssemeijer N, Huisman HJ. Automatic computer-aided detection of prostate cancer based on multiparametric magnetic resonance image analysis. Phys Med Biol 2012;57:1527–42.
[24] Ahmed HU, Arya M, Freeman A, Emberton M. Do low-grade and low-volume prostate cancers bear the hallmarks of malignancy? Lancet Oncol 2012;13.e509–17.
[25] Huang CC, Deng F-M, Kong MX, et al. Re-evaluating the concept of "dominant/index tumor nodule" in multifocal prostate cancer. Virchows Arch 2014;464:589–94.